Analytic description of competitive grain growth

Colin Ophus, Erik J. Luber, and David Mitlin
Department of Chemical and Materials Engineering, University of Alberta, Edmonton, Alberta, Canada
and National Institute for Nanotechnology, Edmonton, Alberta, Canada
(Received 23 July 2009; revised manuscript received 25 November 2009; published 6 January 2010)

We describe an analytic model for polycrystalline thin film growth based on competition between grains with conic geometries. This model is valid for all film thicknesses and is verified using level set simulations in 2+1 dimensions. We study the effects of nonuniform initial grain distributions on growth statistics. These results provide a possible explanation for discrepancies between experimentally measured and theoretical scaling laws.

DOI: 10.1103/PhysRevE.81.011601 PACS number(s): 81.15.Aa, 68.55.J−, 81.10.−h

I. INTRODUCTION

Polycrystalline thin films are important for a wide array of applications including optics, semiconductors, nanomechanical devices and sensors. In addition to variations in bulk material properties, the behavior of polcrystalline materials is strongly influenced by grain morphology [1] and texture [2]. For example, grain structure can influence thin film stresses and etching [3,4], sensitivity and response time of sensors [5], thermal conductivity and surface roughness [6], and semiconductor electrical properties [7,8]. For these reasons it is critical to understand the fundamental processes that govern grain evolution during thin film growth.

Polycrystalline films typically begin as a series of unconnected grains distributed randomly over the substrate surface. The grains expand until they form a continuous film at which point competitive grain growth begins, as originally envisioned by Kolmogorov [9] and van der Drift [10]. Each grain asymptotically evolves toward a kinetic Wulff shape and those grains having more favorable orientations will eventually dominate the surface. If the Schwoebel barrier(s) of one or more low-index crystalline faces is very low, the grain will be extremely faceted and its kinetic Wulff shape will be a simple polyhedron. In the simplest form of faceted polycrystalline thin film growth, the growth velocity of a given facet depends only on its crystallographic orientation.

This type of evolution has been simulated in several recent studies [11–14]. It is also now possible to carefully analyze various aspects of polycrystalline growth both after deposition [15,16] and *in situ* [17]. However, few analytic models are available to analyze faceted polycrystalline growth. The most widely used model was proposed by Thijssen *et al.* in 1992 [18], but this model is only applicable during late-stage growth.

In this study, we derive an analytic model that describes the evolution of a polycrystalline thin film. Like Thijssen, we assume grains can be described geometrically by cones, a comparison elucidated in [14], and construct a model based on the evolution of the angular distribution of cones. However, unlike Thijssen's model, our method is applicable for all times and can be used to describe a larger variety of initial angular distributions.

II. ANALYTIC GROWTH MODEL

A. Initial angular distributions

A conic grain is described with four parameters: the origin in the substrate plane given by coordinates (x_0, y_0) and the primary vector of the cone given by the tilt angle from the substrate normal θ and the angle in the substrate plane ϕ. We make the mean-field-type assumption to ignore the local coordinates of all grains as well as assuming that the distribution of angles ϕ is uniform at all times. Therefore, we need only consider the evolution of the angular density distribution $\rho(\theta)$. Three examples of an angular distribution are shown in Fig. 1.

In a real crystal system, the *fastest growth direction* refers to the most favorable crystallographic orientation(s) of a grain. For conic grains, the fastest growth direction is the vector from the cone origin to its apex. In this study, we arbitrarily set the fastest growth directions to the eight ⟨111⟩ directions; these directions are often observed experimentally in fiber texture films. The simplest initial angular distribution of grains would be a uniform distribution. However, grains will often preferentially nucleate closer to a particular orientation. If this orientation is the same as the fastest growth direction, we refer to the angular distribution as being *biased toward* the fastest growth direction. If however the two orientations are different, we call the angular distribution *biased away* from the fastest growth direction. These three cases are shown as spherical pole figures in Fig. 1; the leftmost case is a primarily ⟨111⟩-oriented initial texture (biased toward), the center case is a uniform initial texture and lastly the rightmost case is a primarily ⟨001⟩-oriented texture (biased away). A ⟨111⟩ direction is shown for reference on each of the plots. In all three cases, the angular grain density as a function of θ (the angle from the nearest fastest growth direction) is calculated by radially integrating around one of the ⟨111⟩ directions, the results of which are also graphed in Fig. 1. The mathematical details of our construction of initial angular distributions is left to Appendix.

B. Model derivation

The analytic model derived here describes the evolution of the angular distribution of grains as the film surface advances. Suppose we have an ensemble of cones with apex

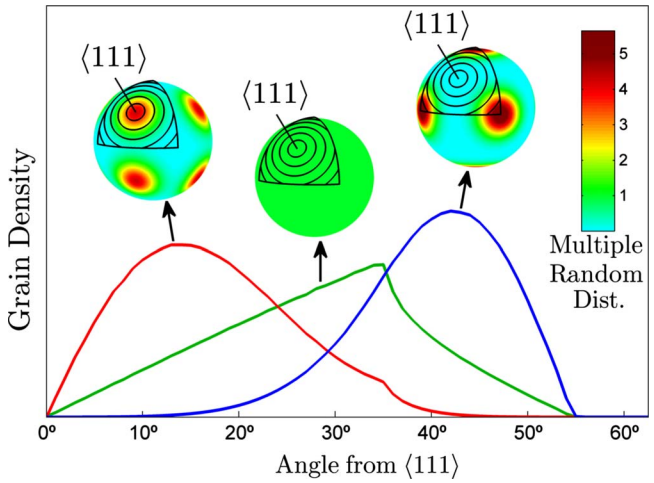

FIG. 1. (Color online) Initial grain orientations distributions from left to right: biased toward fastest growth direction, uniform, and biased away from fastest growth direction. Fastest growth direction and rings showing the direction of integration are plotted on each spherical pole figure.

angle α and angular density distribution $\rho(\theta,t)$. All conic grains will grow at the same velocity, and for convenience, we set the distance from each cone origin to its apex to the growth time t. The advancing surface is composed of grains competing for height, with more favorably oriented grains subsuming those less favorably oriented. To describe the evolution of the surface with time, we must calculate the rate, at which all cones are *deleted* by their neighbors.

First consider two cones having tilt angles $\theta' < \theta$. For convenience we will label the taller cone as cone θ' and the shorter cone as cone θ. Figure 2 shows a deletion event (a cone apex being subsumed by another cone) occurring between time t and $t+\Delta t$. A *deletion plane* is defined parallel to the substrate at the height of the shorter cone's apex. This is the plane, in which the shorter cone's apex collides with the surface of the taller cone.

Geometric considerations dictate that a cone can only ever be deleted by a cone with a more favorable orientation. In order to calculate the probability of this event occurring, we analyze the geometry of the conic section formed by the intersection between the deletion plane and the taller cone.

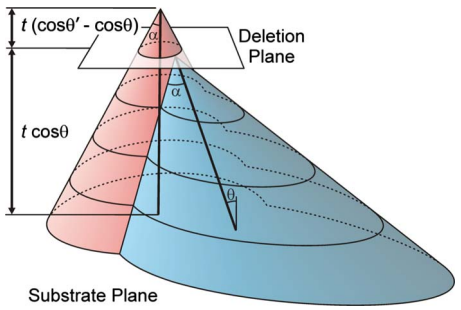

FIG. 2. (Color online) A deletion event between two conic grains at time t in the time interval Δt. Isocontours are shown at different heights. Note that the primary axis of both cones are the same length.

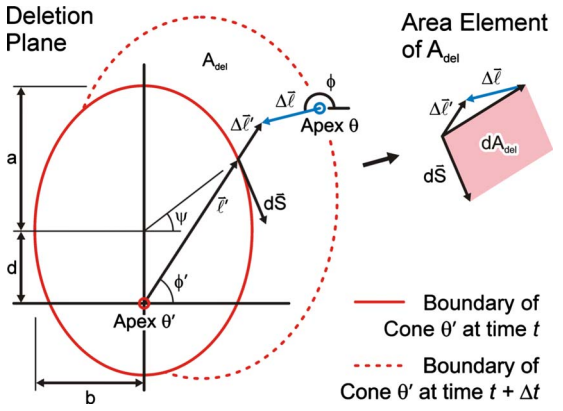

FIG. 3. (Color online) Geometry of a cross-section of the cone with tilt angle θ' in the deletion plane shown in Fig. 2.

Figure 3 shows the geometry of the conic section in the deletion plane. Two different boundaries are shown, the boundary of cone θ' at time t before the deletion event and at time $t+\Delta t$ after the deletion event. The area between these two boundaries defines the deletion area A_{del}. The probability of cone θ' deleting cone θ in any given time interval Δt is simply the area A_{del} divided by the total possible area where the apex of cone θ can be found in.

To calculate A_{del}, we start with the height difference between the two cone apices, $(\cos\theta' - \cos\theta)t$. The major and minor semiaxes a and b, and the distance d from the ellipse center to the apex of cone θ' are all proportional to this height difference and are given by

$$a = \frac{\tan\alpha}{1-\epsilon^2}(\cos\theta' - \cos\theta)t, \tag{1}$$

$$b = \frac{\tan\alpha}{\sqrt{1-\epsilon^2}}(\cos\theta' - \cos\theta)t, \tag{2}$$

$$d = \frac{\tan^2\alpha\tan\theta'}{1-\epsilon^2}(\cos\theta' - \cos\theta)t, \tag{3}$$

where $\epsilon = \sin\theta'/\cos\alpha$ is the eccentricity of the ellipse. Over one time step Δt, the boundary of cone θ' will expand and the apex of cone θ will travel relative to it. The distance $\Delta\mathbf{L}'$ traveled by the elliptic boundary and the distance $\Delta\mathbf{L}$ traveled by the apex of cone θ in the time interval Δt are given by

$$\Delta\mathbf{L}' = \Delta t\frac{\tan\alpha}{1-\epsilon^2}(\cos\theta' - \cos\theta)[\cos\phi', \sin\phi'], \tag{4}$$

$$\Delta\mathbf{L} = \Delta t\sin(\theta)[\cos\phi, \sin\phi], \tag{5}$$

where the direction of these vectors are given by the angles ϕ' and ϕ, respectively. If the boundary is parametrized by $x = b\cos\psi$ and $y = d + a\sin\psi$ where $-\pi < \psi < \pi$ then the arc length segment $d\mathbf{S}$ and $\Delta\mathbf{L}'$ can be written as

$$d\mathbf{S} = d\psi[b\sin\psi', -a\cos\psi'], \tag{6}$$

$$\Delta \mathbf{L}' = \frac{\Delta t}{t}(\cos\,\theta' - \cos\,\theta)[b\,\cos\,\psi, d + a\,\sin\,\psi]. \quad (7)$$

As shown in Fig. 3 the differential deletion zone is a parallelogram having an area dA_{del} given by

$$dA_{del} = \left[\sin\,\theta(a\,\cos\,\psi\,\cos\,\phi + b\,\sin\,\psi\,\sin\,\phi) + \frac{b}{t}(a + d\,\sin\,\psi)\right]\Delta t d\psi. \quad (8)$$

Because ψ varies from $-\pi$ to π we can introduce an arbitrary phase shift and rewrite Eq. (8) as

$$dA_{del} = \left[\sin\,\theta\,\cos\,\phi\sqrt{a^2\,\cos^2\,\psi + b^2\,\sin^2\,\psi} + \frac{b}{t}(a + d\,\sin\,\psi)\right]\Delta t d\psi. \quad (9)$$

To find the total deletion area A_{del} we must integrate over ψ and average over all ϕ, where $dA_{del} > 0$ giving

$$A_{del} = \frac{2\Delta t}{\pi}\int_{-\pi/2}^{\pi/2}\int_{0}^{\cos^{-1} w}\left[\sin\,\theta\,\cos\,\phi\sqrt{a^2\,\cos^2\,\psi + b^2\,\sin^2\,\psi} + \frac{b}{t}(a + d\,\sin\,\psi)\right]d\phi d\psi, \quad (10)$$

where

$$w = -\frac{b(a + d\,\sin\,\psi)}{t\,\sin\,\theta\sqrt{a^2\,\cos^2\,\psi + b^2\,\sin^2\,\psi}}. \quad (11)$$

Integrating in ϕ we obtain the expression

$$A_{del} = \frac{2\Delta t}{\pi}\int_{-\pi/2}^{\pi/2}\left[\sin\,\theta\sqrt{1 - w^2}\sqrt{a^2\,\cos^2\,\psi + b^2\,\sin^2\,\psi} + \cos^{-1}(w)\frac{b}{t}(a + d\,\sin\,\psi)\right]d\psi. \quad (12)$$

This equation is numerically evaluated for all values of θ and θ' of interest for a given value of α. To evolve the angular density distribution $\rho(\theta, t)$ over all time, we weight the area of deletion by the angular density distribution to calculate the probability of deletion for each value of θ in the time interval Δt. The new density distribution after this time interval can be calculated by multiplying the old distribution by the survival probability, equal to one minus the probability of deletion, i.e.,

$$\frac{\rho(\theta)|_{t+\Delta t}}{\rho(\theta)|_t} = 1 - \int_0^{\theta} A_{del}(\theta, \theta', \alpha)\rho(\theta')|_t d\theta'. \quad (13)$$

Note that the upper bound of the integral is θ, reflecting the physical rule that a cone can only be deleted by a cone with a more favorable orientation (one with a lower θ value). To calculate the evolution of an angular distribution function, Eq. (12) is solved first for all θ and θ' values of interest and then that data is used evolve the distribution using Eq. (13).

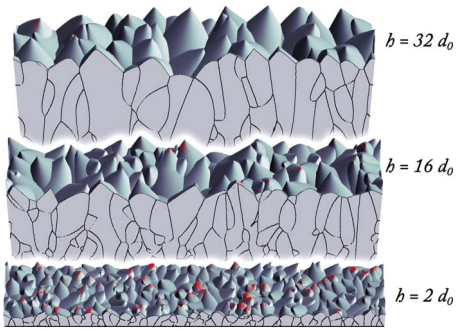

FIG. 4. (Color online) Examples of competitive conic grain growth from level set simulations at various thicknesses. Surfaces are shaded by x-direction slope and cross-sectional slices also shown. Potential deletion zones marked in red. Animated version available online in supplementary materials (Ref. [20]).

III. MODEL VALIDATION

A. 2+1D simulation of conic grains

To test the analytic model given by Eqs. (1)–(3) and (11)–(13), we have used level set simulations of competitive conic grain growth. The conic surface of each grain is described by a four-dimensional implicit function. At each time step all surfaces are advanced and a 2+1-dimensional surface $z(x, y)$ is calculated from the union of all cones. When a cone apex is subsumed into the surface, the cone ceases to grow. An example simulation is shown in Fig. 4 of cones with $\alpha = 30°$ and a uniform distribution of tilt angles up to a cutoff of $\theta_c = 45°$. More details on the simulation methodology are given in [11,14].

The mean heights of the simulation surfaces shown in Fig. 4 are given in units of initial grain spacing d_0, defined as the square root of mean initial grain area A_0 for convenience. Survival probability P is measured by dividing the number of surviving grains by the number of initial grains. Figure 4 clearly shows that P decreases monotonically with film thickness h. Note that mean thickness is asymptoting toward time (defined as the length of the primary vector of each cone), which approximately follows the relationship $h = t - 1/2\,\tan\,\alpha\sqrt{P}$.

B. Comparison of model to simulation

A comparison of grain orientation distributions between level set simulations of 10^6 cones and the analytic model, with both having $\alpha = 30°$, is shown in Fig. 5 for the three cases described in Fig. 1. The agreement is excellent over all times, validating the analytic model.

It is important to point out that no mean-field assumptions were used in the level set simulations. Because the simulation and the model agree, our decision to neglect local grain correlations in the analytic model is validated. Even if local angular or positional correlations of grains do occur, they do not affect the global evolution of the surface in any meaningful way.

IV. ANALYSIS OF GRAIN GROWTH MODEL

A. Self-similarity of distributions

The angular distributions shown in Fig. 5 display remarkable self-similarity between different thicknesses. Thijssen *et*

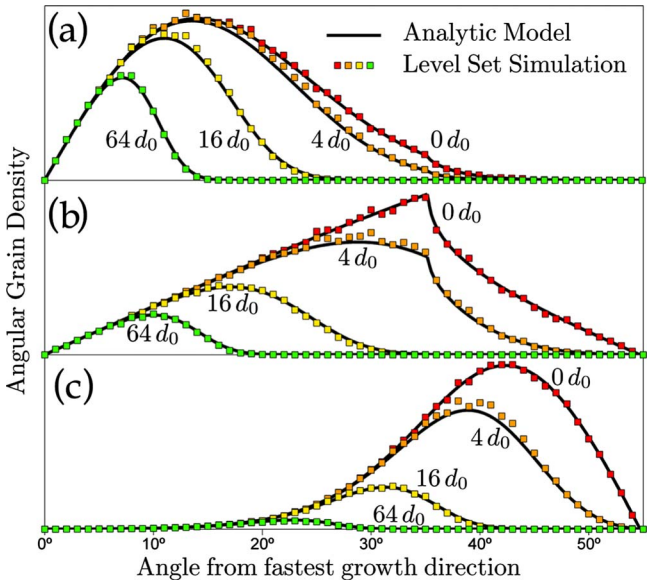

FIG. 5. (Color online) Comparison of the grain distribution at four different film thicknesses between analytic growth model and level set simulation for the cases where the initial distribution is (a) biased toward the fastest growth direction, (b) uniform, and (c) biased away from the fastest growth direction.

al. suggested that $\log(\rho(\theta,t)/\theta) \propto t^2\theta^5$ in late-stage film growth [18]. We derive an exact expression for the asymptotic angular distribution as follows. Each of the angular distributions seen in Fig. 5 asymptotes toward a constant slope,

$$\eta = \left.\frac{\partial \rho}{\partial \theta}\right|_{\theta \to 0}. \tag{14}$$

This slope is proportional to the number of grains initially oriented in the fastest growth direction. Note that this value must be estimated or measured experimentally for a given initial angular distribution. The asymptotic form of the angular distribution is given by

$$\rho(\theta,t) = \eta\theta \exp\left[-k\left(\frac{t}{\tau}\right)^2 \theta^5\right], \tag{15}$$

where k is a scaling constant and τ is the cross-over thickness into late-stage, or self-similar behavior. To solve for k, we note that the grain probability of survival is unity at $t=\tau$. Integrating Eq. (15) from 0 to ∞ when $t=\tau$ gives $k=[\eta\Gamma(\frac{2}{5})/5]^{5/2}$, where Γ is the gamma function. The angular distribution at late times is therefore

$$\rho(\theta,t) = \eta\theta \exp\left\{-\left[\frac{\eta\Gamma\left(\frac{2}{5}\right)}{5}\right]^{5/2}\left(\frac{t}{\tau}\right)^2 \theta^5\right\}, \tag{16}$$

which agrees with distributions generated by both numerical iteration of Eq. (13) and level set simulations.

B. Scaling laws

The goal of our analytic growth model is to predict morphological statistics for this type of polycrystalline film growth. Most statistical measures in thin film growth follow power laws with thickness (or equivalently time, for constant deposition rate). Survival probability P is calculated by integrating the angular density distribution

$$P(t) = \int_0^{\pi/2} \rho(\theta,t)\, d\theta. \tag{17}$$

Inserting Eq. (16) into Eq. (17) gives

$$P = (t/\tau)^{-4/5}. \tag{18}$$

Other growth statistics such as expectation value of grain area $\langle A\rangle$ and the root-mean-square (rms) surface roughness σ have simple relationships to the grain survival probability, the derivations of which are given in the appendix of [14]. From our model we have calculated scaling laws for $\langle A\rangle$ and σ at late-stage growth of

$$\langle A\rangle = (t/\tau)^{4/5}, \tag{19}$$

$$\sigma = \frac{1}{\tan\alpha}\sqrt{\frac{1}{\pi} - \frac{1}{4}}(t/\tau)^{2/5}. \tag{20}$$

Our calculated exponents match those predicted by Thijssen for late-stage growth [18]. However, our model can also predict the value of crossover thickness τ, based only on the cone angle α and the asymptotic value of the slope of the distribution at small angles η. This is achieved by expanding both sides of Eq. (13) and using the small angle approximation for all θ and θ' terms. Note that in late-stage growth only the first term in Eq. (12) needs to be considered.

$$\frac{e^{-\{[\eta\Gamma(2/5)]/5\}^{5/2}[(t+\Delta t)/\tau]^2\theta^5}}{e^{-\{[\eta\Gamma(2/5)]/5\}^{5/2}(t/\tau)^2\theta^5}} = 1 - 2\Delta t\,\eta\int_0^\theta a\,\sin\,\theta\theta'\,d\theta',$$

$$1 - \left[\frac{\eta\Gamma\left(\frac{2}{5}\right)}{5}\right]^{5/2}\frac{2t\Delta t}{\tau^2}\theta^5 = 1 - t\Delta t\,\eta\tan\alpha\frac{\theta^5}{4},$$

$$\tau = \sqrt{8}\left[\frac{\Gamma\left(\frac{2}{5}\right)}{5}\right]^{5/4}\frac{\eta^{3/4}}{\sqrt{\tan\alpha}}. \tag{21}$$

Noting that the coefficient of Eq. (21) is approximately unity gives

$$\tau = \frac{\eta^{3/4}}{\sqrt{\tan\alpha}}. \tag{22}$$

Equation (22) was confirmed by comparing its predictions to the crossover thicknesses observed in the analytic model for many values of α and η.

C. Effect of nonuniform initial angular distributions

We now analyze the effect that biasing the initial growth direction toward or away from the fastest growth direction has on the growth statistics. Figure 6 shows rms surface

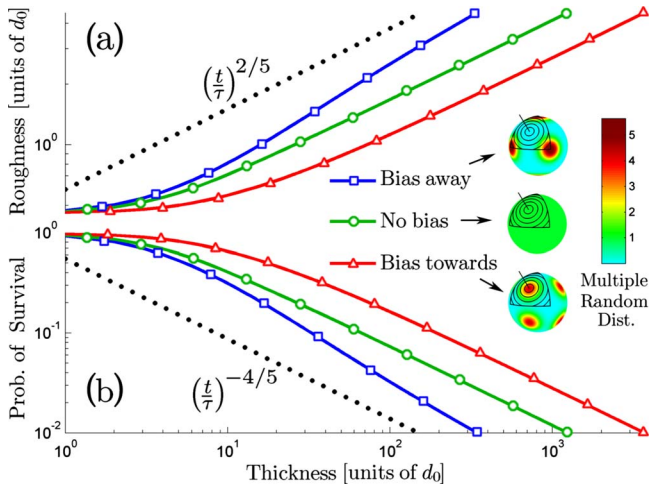

FIG. 6. (Color online) (a) rms surface roughness and (b) probability of grain survival calculated from the analytic growth model for the three cases described in Fig. 1. Power laws are shown in both graphs as dotted lines.

roughness and probability of grain survival versus film thickness for the three cases described above. All three cases asymptote toward the expected power laws as $t \to \infty$. However, biasing the initial grain distribution toward the fastest growth direction delays deletion of grains, leading to longer survival times. In this case the surface is much smoother because the mean peak to peak distances are dramatically reduced. Biasing the growth direction away from the fastest growth direction has the opposite effect on both statistical measures. These effects manifest in the thickness range from roughly $1 < h < 1000 d_0$.

Interestingly, the studies performed in [15,19] found power law exponents for roughness and grain diameter in excess of the predicted value of 0.4. This study suggests that an initial nucleation of grains with texture biased away from the fastest growth direction could be responsible for the observed power law deviations. And indeed, an initial texture bias toward ⟨001⟩ was observed in those studies compared to a fastest grain growth direction near ⟨111⟩. To confirm our explanation, careful measurements of the initial grain angular distributions will be required.

V. CONCLUSION

To summarize, we have derived an analytic model for polycrystalline grain growth based on conic grain geometries. This model showed excellent agreement compared to level set simulations of conic surfaces and the results can be computed in a much shorter time span. Three initial angular grain density distributions were analyzed. When the distribution was biased toward the fastest growth direction, the probability of survival for each grain is increased and the surface roughness is decreased compared to a uniform initial distribution. When the distribution is biased away from the growth direction, the opposite trends are observed. These results underscore the importance of the initial grain distribution when analyzing polycrystalline thin film growth. Finally, the cross-over thickness into late-stage growth is predicted with a simple analytic expression.

ACKNOWLEDGMENTS

This study was funded by the Natural Sciences and Engineering Research Council of Canada and Alberta Ingenuity. The authors would also like to thank Brian C. Olsen for technical help and Andrew J. Murray for his insight into the mechanisms of grain deletion.

APPENDIX: INITIAL TEXTURE DISTRIBUTIONS

In this work the orientation distribution functions (ODFs) $g(\theta, \phi)$, were constructed using the following equation

$$g(\theta,\phi) = \frac{2N+1}{4\pi\left(\sum_{i=1}^{P} w_i\right)} \sum_{i=1}^{P} w_i |\hat{\mathbf{u}}_i \cdot \hat{\mathbf{r}}(\theta,\phi)|^{2N}, \tag{A1}$$

where $\hat{\mathbf{u}}_i$ is a unit vector in the direction of the ith pole, $\hat{\mathbf{r}}(\theta, \phi)$ is the unit position vector in spherical coordinates, w_i is the relative weighting of the ith pole, P is the total number of poles and N determines the degree of texturing. Note that this expression assumes an equal weighting of each pole and its antiparallel direction; therefore, there is no need to specify both $\hat{\mathbf{u}}_i$ and $-\hat{\mathbf{u}}_i$ for any given i. The ⟨111⟩-oriented ODF is constructed using all four ⟨111⟩ directions ($\hat{\mathbf{u}}_i$) with equal weighting (w_i) and $N=8$. The ⟨001⟩ oriented ODF is constructed using all three ⟨001⟩ directions with equal weighting and $N=8$. The uniform ODF is constructed using a single pole with $N=0$.

The N parameter is used to control the sharpness of the texture. When $N=0$, the distribution has random texture, as N is increased the texture becomes progressively sharper. The N parameter can be directly related to more commonly used metrics to describe the degree of texture, such as the texture index J,

$$J = 4\pi \sum_{l=0}^{\infty} \sum_{m=-l}^{m=l} |Q_l^m|^2, \tag{A2}$$

where Q_l^m are the Fourier coefficients of the spherical harmonic expansion of the ODF. For a uniform texture distribution $J=1$ and as the texture sharpens J takes on larger values. Applying Parseval's theorem, the texture factor can be expressed equivalently as

$$J = 4\pi \int_0^{2\pi} \int_0^{\pi} g^2(\theta,\phi) \sin\theta \, d\theta \, d\phi. \tag{A3}$$

Using Eqs. (A1) and (A3) an exact expression for the texture index can be derived for an ODF consisting of ⟨001⟩ poles, given by

$$J = \left(1 + \frac{4N^2}{4N+1}\right) \frac{\sum_{ij} w_i w_j \left[\delta_{ij} + (1-\delta_{ij}) \frac{2\Gamma^2(N+1/2)}{\sqrt{\pi}\Gamma(2N+1/2)}\right]}{\left(\sum w_i\right)^2}. \tag{A4}$$

As N is increased beyond unity the second term within the brackets exponentially approaches zero, giving the following relation

$$J \simeq (N+1) \frac{\sum w_i^2}{\left(\sum w_i\right)^2}. \tag{A5}$$

Moreover, it can be shown that Eq. (A5) is valid for any number of poles pointing in arbitrary directions provided that N is sufficiently large.

[1] I. Petrov, P. B. Barna, L. Hultman, and J. E. Greene, J. Vac. Sci. Technol. A **21**, S117 (2003).
[2] H. R. Wenk and P. Van Houtte, Rep. Prog. Phys. **67**, 1367 (2004).
[3] V. Cimalla, J. Pezoldt, and O. Ambacher, J. Phys. D **40**, 6386 (2007).
[4] J. Leib, R. Monig, and C. V. Thompson, Phys. Rev. Lett. **102**, 256101 (2009).
[5] G Korotcenkov, Mater. Sci. Eng. R. **61**, 1 (2008).
[6] D. Das and R. N. Singh, Int. Mater. Rev. **52**, 29 (2007).
[7] F. Greuter and G. Blatter, Semicond. Sci. Technol. **5**, 111 (1990).
[8] Y. Yan, R. Noufi, and M. M. Al-Jassim, Phys. Rev. Lett. **96**, 205501 (2006).
[9] A. N. Kolmogorov, Bull. Acad. Sci. USSR, Phys. Ser. (Engl. Transl.) **1**, 355 (1937).
[10] A. van der Drift, Philips J. Res. **22**, 267 (1967).
[11] P. Smereka, X. Li, G. Russo, and D. J. Srolovitz, Acta Mater. **53**, 1191 (2005).
[12] O. Nilsen, O. B. Karlsen, A. Kjekshus, and H. Fjellvg, J. Cryst. Growth **308**, 366 (2007).
[13] S. A. Norris and S. J. Watson, Acta Mater. **55**, 6444 (2007).
[14] C. Ophus, E. Luber, and D. Mitlin, Acta Mater. **57**, 1327 (2009).
[15] E. Spiecker, V. Radmilovic, and U. Dahmen, Acta Mater. **55**, 3521 (2007).
[16] C. Lim, J. Lee, and J. Hanna, Thin Solid Films **517**, 2627 (2009).
[17] M. J. Rost, Phys. Rev. Lett. **99**, 266101 (2007).
[18] J. M. Thijssen, H. J. F. Knops, and A. J. Dammers, Phys. Rev. B **45**, 8650 (1992).
[19] V. Radmilovic, U. Dahmen, D. Gao, C. R. Stoldt, C. Carraro, and R. Maboudian, Diamond Relat. Mater. **16**, 74 (2007).
[20] See supplementary material at http://link.aps.org/supplemental/10.1103/PhysRevE.81.011601 for animated movie of a polycrystalline grain growth simulation.